Supplementary Section to "Motor step size and ATP coupling efficiency of the dsDNA translocase EcoR124I"

Ralf Seidel, Joost G.P. Bloom, Cees Dekker and Mark D. Szczelkun

Supplementary Methods

Preparation, characterization and precision of the PBP phosphate sensor

The phosphate release assay relies on a phosphate binding protein (PBP) covalently linked to a coumarin derivative (MDCC) that exhibits fluorescence that is sensitive to the specific, reversible association of P_i (Webb 2003; 2007). The use of MDCC-PBP as a phosphate sensor has been extensively characterised (Brune et al., 2001) and used widely in the study of motor proteins, including helicases (*e.g.*, Dillingham et al., 2000; Martinez-Senac and Webb, 2005; Tomko et al., 2007). One of the advantages of the MDCC-PBP sensor is that Pi binding is rapid and tight: at 5 μM MDCC-PBP (pH 7.0, 5 °C), the observed rate of fluorescence change has a limiting rate of 150 /s and a K_D of 0.1 μM (Webb 2003). Because we measured a steady-state accumulation of P_i, the observed rates were not limited by the K_D and the signal was linear with P_i concentration at all temperatures (see below). The maximal ATPase rates measured under our experimental conditions (≤1200 μM ATP) were not rate-limited by the Pi-binding rate (Webb, 2003).

The purified and labelled sensor was characterised initially as described by Webb (2003) (**Fig. S1**). We chose to use 12 μM PBP in subsequent assays to allow reliable linear measurement of up to 6 μM Pi (all steady-state fits were made in the range of ≤5 μM P_i released). Calibration of the stopped flow was carried out for each temperature by titrating known concentrations of a P_i standard (Webb, 2003; **Fig. S2; Table S1**). In brief, Syringes "C" and "D" were filled with 5 μM MDCC-PBP in Reaction Buffer (50 mM Tris-Cl, pH 8.0, 10 mM $MgCl_2$, 1 mM DTT). Equal volumes (50 μl) of C and D were mixed and the solution monitored for 60 s (**Fig. S2A**). 0.5 μM aliquots of the P_i standard (VWR International Ltd, Lutterworth, UK) were added to each syringe and the fluorescence re-measured each time after pushing the new solution into the observation chamber. The PMT response at each concentration of P_i

was calculated from the average of two traces. The data was fitted to a linear relationship (**Fig. S2B**) to give V/μM Pi (**Table S1**).

To ensure that the MDCC-PBP sensor accurately returns the true ATPase rate, we compared the kinetics of P_i production measured using the sensor with the kinetics of ADP production measured using a hand-quenched assay with radioactive (α-^{32}P)-ATP. We performed the assays at 15 °C and 96 μM ATP to allow sufficient time for initiation and quenching by hand-mixing. The phosphate release assay was carried out as in Materials and Methods, Main Section. The radioactive assay was modified from Pederson and Catterall (1979) and was carried out as follows: Two samples were prepared in Reaction Buffer and pre-incubated at 15.0±0.1 °C in a Grant LTD6G waterbath: Sample "A" contained 1 nM ApaI-linearised pLKS5, 120 nM MTase and 400 nM HsdR; Sample "B" contained 192 μM ATP [comprising 3.3 nM (α-^{32}P)-ATP; PerkinElmer Life And Analytical Sciences, Inc., Waltham, MA]. Reactions were initiated by mixing equal volumes of samples A and B to give final reaction conditions equivalent to those in the phosphate release assay. Reactions were allowed to proceed for a defined time interval and then quenched by mixing with 0.5 volumes of 0.5 M EDTA (pH 8.0) (Firman and Szczelkun, 2000). The error from uncertainties in the mixing protocol are ±1 s. The (α-^{32}P)-ATP and (α-^{32}P)-ADP were separated by thin layer chromatography (TLC) on 20 × 20 cm PEI-cellulose F-coated plastic sheets (Merck, Germany) developed in 0.75 M KH_2PO_4 (pH 4.4) at 20 °C. The sheets were dried and the amounts of (α-^{32}P)-ATP and (α-^{32}P)-ADP determined using a Typhoon phosphorimager and ImageQuant TL v2005 (GE Healthcare UK Ltd). Each lane was corrected for the background contamination of (α-^{32}P)-ADP. Enzyme-independent ATP hydrolysis was negligible over this time scale (data not shown). There is good agreement between the total amount of ATP hydrolysed as measured by release of P_i (stopped flow PBP assay) or ADP (hand-mixed radioactive assay) (**Fig. S3**).

Sources of error in the ensemble experiments

There are two sorts of error in our ensemble experiments: Statistical/random errors and systematic errors. The statistical errors arise due to mechanical or human variation in experimental procedures (e.g., temperature variations, inaccuracy in pipetting, *etc*). These errors apply to both the triplex and ATPase assays and add to the scatter of the data. Additional random errors arise in the ATPase assays due to the

calibration of the stopped flow using the P_i standard. The systematic errors arise due to assumptions about the experimental conditions, the extent of which are constant and proportional throughout the experiments. These affect the phosphate release assay only. The source and magnitude of the errors in each experiment are discussed below.

Principle sources of statistical error

1. Pipetting - Using the Gilson Pipetman range of pipettes (P2 – P1000), errors from dispensing volumes into the reactions are ≤2% (assuming the correct choice of pipette for each volume: www.gilson.com).

2. Temperature - The temperature of the SF61-DX2 stopped flow is controlled by a Thermo Scientific NESLAB RTE-7 refrigerated circulating bath with a temperature accuracy of ±0.01 ºC. Since this systematic error is the same for both the triplex and ATPase assays, we need not consider it. The temperature of the stopped-flow manifold was also monitored directly, giving an apparent accuracy of ±0.1 ºC. Therefore, there could be random fluctuations within these limits. With $Q_{10} = 2$ [$Q_{10} = (R_2/R_1)^{(10/T_2-T_1)}$, where R_1 is the rate at the lower temperature T_1 and R_2 is the rate at the higher temperature T_1], a fluctuation of ±0.1 ºC gives an error in the ATPase and translocase rates of <0.7 %.

3. Phosphate calibration – In order to calibrate the response of the phosphate sensor in the stopped flow, the system was calibrated during each experiment by titrating known concentrations of P_i (see text above; **Fig. S2; Table S1**). The error range for these calibration curves was 0.5 – 2.6% as judged from the goodness of the linear fit. No systematic error with temperature was observed. The calibration error is larger than the systematic error in the concentration of the P_i standard (0.5%).

Principle sources of systematic error

The determination of the rate of ATP hydrolysis per HsdR in the phosphate release assay relies on an accurate knowledge of the concentration of the steady-state translocating species that contribute to the accumulation of P_i (see Main Section and **Figs. S4-S6**). Consequently, the principle sources of systematic error are from uncertainties in the DNA concentration (which defines the maximum possible concentration of translocating species) and in the absolute occupancy of that steady-

state. In comparison, the determination of k_{step} values from the triplex assay is robust and is independent of concentration effects (McClelland et al., 2005). The data from the triplex assay compares very well with independently-determined values from the single molecule experiments (see **Fig S10**; Seidel et al., 2005).

1. Accuracy of the DNA concentration - The concentration of translocating species is calculated from the concentration of DNA used in the reactions. Hence, the accuracy of the DNA concentration will directly affect the accuracy of the observed ATPase rate. All DNA used in the ensemble studies was highly-purified by density gradient centrifugation in CsCl-ethidium bromide (Vipond et al., 1995). DNA concentration was measured by absorbance at 260 nm in a Perkin Elmer Lambda 14 spectrophotometer using an average extinction coefficient for dsDNA of 0.02 ml/μg/cm (Sambrook and Russell, 2001). This value is universally used in the study of large DNA substrates. For small single-stranded oligonucleotides (<60 nt), a number of alternative methods can be used to determine the concentration. Extinction coefficients can be predicted by the weighted sum of mononucleotide extinction coefficients (Sambrook and Russell, 2001) or by nearest-neighbour methods using mono- and dinucleotide addivity rules (Cantor et al., 1970). Both methods are reproducible but are subject to errors in the published extinction constant values and can show systematic variations of 15-25% (Cavaluzzi and Borer, 2004). These methods are even more unreliable if applied to dsDNA. More accurate DNA concentrations can be ascertained by general phosphate analysis (Murphy and Trapane, 1996) or by hydrolysis with a mixture of nucleases (Kallansrud and Ward, 1996). These methods are likely to be accurate to within 2-5% using high DNA concentrations (>10 μM; Cavaluzzi and Borer, 2004), assuming that digestion is complete and that no chemical modification has occurred. The most accurate method (to within <1% and limited by pipetting errors) is to use ^{1}H-NMR (Cavaluzzi et al., 2002). However, this requires even higher concentrations (> 1 mM) and is limited to relatively small biomolecules (10-20 kDa) that have sharp, non-overlapping NMR signals. Because of the length of the dsDNA used in this study (~7.6 kbp) and the relatively low yields from the plasmid preparations (~ 50 pmoles), none of the above methods would be applicable here. A recent study by Cavaluzzi and Borer, (2004), however, has shown that the approximated mean extinction coefficients are as accurate for random, non-repetitive sequences as other methods, with an error in the

accuracy of less than ±5%. Due to the long DNA templates used in the study there is an excellent even distribution of all nearest neighbour base pairs in good approximation of randomly-mixed DNA sequences. We therefore consider the error in the concentrations of our DNA to be ±5%. We furthermore note that even assuming an error as large as 10% in the DNA concentration, the conclusions of the paper are not affected.

In correcting for the background HsdR ATPase rate, we used a non-specific DNA that had 98% sequence-identity to the specific DNA. The relative concentrations of the two DNA were checked by ethidium bromide fluorescence following agarose gel electrophoresis and shown to be matched to within 1%.

2. Occupancy of the steady-state - In using the DNA concentration as a measure of the number of translocating motor species, we assume that the DNA is both saturated with enzyme and that all enzymes are translocating (*i.e.*, the steady-state is fully occupied). The first assumption was validated by using concentrations of MTase and HsdR in excess of the DNA (**Fig. 1B**). The second assumption depends on the kinetic parameters of the accepted EcoR124I translocation cycle (Seidel et al., 2005; **Fig. 1A and S4A**). We simulated this scheme using values determined previously (Seidel et al., 2005) and could show that the profiles obtained are similar to those observed in the ATPase assay (**Fig. S4B**). These profiles can be approximated by a single exponential approach to the steady-state (**Fig. S4C**). Deviation of the empirical data from a single exponential relationship is suggestive of additional kinetic steps during initiation (**Fig. S5**). We therefore used a direct linear fit of the steady-state to measure the apparent ATPase rate (**Eqn. 3**; see Main Section)

Given the EcoR124I translocation cycle (**Fig. S6A**), there is a finite possibility that following initiation of translocation, the HsdR will dissociate from the DNA and MTase. (We avoided the additional complication of DNA end effects by using long substrates where the HsdRs were unlikely to reach an end during the course of the measured reaction.) Re-entry of an HsdR back into the steady-state then relies on a second order association with the DNA-bound MTase followed by a first order initiation step (Seidel et al., 2005). Under our experimental conditions, the association of the HsdR and MTase is not rate-limiting. However, the initiation step is sufficiently slow that following dissociation of an HsdR, there is a significant delay before translocation is re-established. Consequently, the steady-state is sub-saturated (**Fig.**

S6B), which leads to an underestimation of the ATPase rate. Based on our previously determined kinetic parameters (Seidel et al., 2005), we can rather precisely determine the error in the observed steady-state ATPase rate as ~+5% (**Fig. S6B and S6C**). This error is asymmetric as the occupancy of the steady-state cannot exceed 100%.

For the determination of K_M and V_{max} in both **Figs. 1E and 2C**, the statistical errors are smaller than the scatter in the data points (<3% for the triplex data; <6% for the phosphate release data). Since the scatter makes a greater contribution to the statistics of the fit, the fitting to **Eqn. 4** was not weighted to the statistical errors. For the ATPase data, the systematic errors will affect all data points to the same extent and with the same sign and therefore were not used to weight the fit. For the Arrhenius plots in **Fig. 3A**, the same considerations apply and fitting to **Eqn. 1** was not weighted to either statistical or systematic errors.

Where the systematic errors in the ATPase data become important is in the calculation of the coupling ratios in **Fig. 3C**. We first calculated the ratios from the k_{ATP} and k_{step} values independent of any statistical errors, the scatter in the data being more significant. Because the resulting ratios show no systematic variation with either ATP concentration or temperature, we then calculated the average coupling ratio and 95% confidence interval providing an S.E.M. of 4%. Finally, we added the total systematic error from the ATPase values (+11% and -6%, see above) to the statistical error to give a final value that quantifies the precision of the sample mean (1.26 + 0.19/ -0.13 ATP/bp; **Fig. 3C**). We can therefore state with a high degree of confidence that the true coupling ratio lies above 1 in the range of 1.1 – 1.5 ATP/bp.

Description of the Monte-Carlo simulations

Apparent step size as a function of uncoupled steps

In order to determine the influence of uncoupled steps (see **Fig. 5D**) on our power-spectrum based step-size determination, we carried out computer-based Monte-Carlo simulations. We simulated time traces of motor movement by choosing a certain minimal time increment, ΔT, which was at least 100 times shorter than the average time between two motor steps, or in other words by choosing a simulation frequency $1/\Delta T$, which is at least 100 times faster than the productive stepping rate of a single

motor $k_{ATP,productive}$ (see Fig. 5c for rate descriptions). We were then evaluating a large number of sequential time points (typically 1000s for 500 bp/s stepping rate), which were separated by ΔT. Using computer-generated random numbers, at each time point, each single motor was randomly allowed to make a single step with a certain chance given by $k_{ATP,productive}*\Delta T$. Uncoupling was introduced by allowing each step to be productive, which results in a change of its forward position of 1 bp (the true step size), or non-productive, which does not change the motor position. If a non-productive step was made the chance per time point for a subsequent step was $k_{ATP,non-productive}*\Delta T$. The chance to make a non-productive step once a step is being made is given by $k_{uncouple}/(k_{uncouple} + k_{ATP,productive})$, which results in a coupling ratio of <ATP/bp> of $(k_{uncouple} + k_{ATP,productive})/k_{ATP,productive}$. After running the simulation for typically 1000 s, the generated time trace was treated in much the same way as the experimental time trace (see Methods). The linear slope of the trace was removed, the power spectrum of the full trace was calculated, smoothed by averaging over 5 subsequent points using a sliding window and then fitted using **Eqn. 2** (see Main Section) without background correction. This provides the apparent step size. Simulations were carried out for different coupling ratios <ATP/bp> and different ratios $k_{ATP,productive}/k_{ATP,non-productive}$. For each set of parameters, the simulation was repeated 10 times and the step sizes obtained were averaged.

The results shown (**Fig. 6B**) were for obtained for $k_{ATP,productive}$ = 500 bp/s and the simultaneous action of two independent motors. However, we note that identical results were obtained within error for different $k_{ATP,productive}$ values and for simulations considering only a single motor.

Apparent step size within the clockwork model

The simulation of time traces based on the clockwork model (see **Fig. 5C**) was carried out analogously to the uncoupled model described above by allowing a 1 bp step at each time point with a probability of $k_{fast}*\Delta T$. After n steps have been made, a pause is introduced by lowering the probability to make the next step to $k_{slow}*\Delta T$. After this pause a new cycle of n fast, 1 bp steps is then initiated. The apparent step size was determined as explained above. Simulations were carried out for different n values and for different ratios between k_{fast} and k_{slow} (**Fig. 6A**).

Supplementary References

Brune M, Corrie JE, Webb MR (2001) A fluorescent sensor of the phosphorylation state of nucleoside diphosphate kinase and its use to monitor nucleoside diphosphate concentrations in real time. *Biochemistry* **40**:5087-5094.

Cantor CR, Warshaw MM, Shapiro H (1970) Oligonucleotide interactions. 3. Circular dichroism studies of the conformation of deoxyoligonucleotides. *Biopolymers* **9**:1059-1077

Cavaluzzi MJ, Borer PN (2004) Revised UV extinction coefficients for nucleoside-5'-monophosphates and unpaired DNA and RNA. *Nucleic Acids Res.* **32:** e13

Cavaluzzi MJ, Kerwood DJ, Borer PN (2002) Accurate nucleic acid concentrations by nuclear magnetic resonance. *Anal. Biochem.* **308**: 373-380

Dillingham MS, Wigley DB, Webb MR (2000) Demonstration of unidirectional single-stranded DNA translocation by PcrA helicase: measurement of step size and translocation speed. *Biochemistry* **39**, 205-212.

Firman K, Szczelkun MD (2000) Measuring motion on DNA by the type I restriction endonuclease EcoR124I using triplex displacement. *EMBO J.* **19:** 2094-2102

Frieden C (1979) Slow transitions and hysteretic behavior in enzymes. *Annu. Rev. Biochem.* **48:** 471-489

Kallansrud G, Ward B (1996) A comparison of measured and calculated single- and double-stranded oligodeoxynucleotide extinction coefficients. *Anal. Biochem*. **236**: 134-138

McClelland SE, Dryden DTF, Szczelkun MD (2005) Continuous assays for DNA translocation using fluorescent triplex dissociation: application to type I restriction endonucleases. *J. Mol. Biol.* **348:** 895-915

Martinez-Senac MM, Webb MR (2005) Mechanism of translocation and kinetics of DNA unwinding by the helicase RecG. *Biochemistry* **44**:16967-16976.

Murphy JH, Trapane TL (1996) Concentration and extinction coefficient determination for oligonucleotides and analogs using a general phosphate analysis. *Anal. Biochem.* **240**, 273-282.

Pedersen PL, Catterall WA (1979) The use of thin-layer chromatography on poly(ethyleneimine) cellulose to facilitate assays of ATP-ADP exchange, ATP-Pi

exchange, adenylate kinase, and nucleoside diphosphokinase activity. *Methods Enzymol*. **55**:283-289

Sambrook JC, Russell DW (2001) Molecular Cloning: A Laboratory Manual. Cold Spring Harbor Laboratory Press, Cold Spring Harbor, NY

Seidel R, van Noort J, van der Scheer C, Bloom JG, Dekker NH, Dutta CF, Blundell A, Robinson T, Firman K, Dekker C (2004) Real-time observation of DNA translocation by the type I restriction modification enzyme EcoR124I. *Nat. Struct. Mol. Biol.* **11:** 838-843

Seidel R, Bloom JG, van Noort J, Dutta CF, Dekker NH, Firman K, Szczelkun MD, Dekker C (2005) Dynamics of initiation, termination and reinitiation of DNA translocation by the motor protein EcoR124I. *EMBO J.* **24:** 4188-4197

Tomko EJ, Fischer CJ, Niedziela-Majka A, Lohman TM (2007) A nonuniform stepping mechanism for E. coli UvrD monomer translocation along single-stranded DNA. *Mol. Cell* **26**:335-347

Vipond IB, Baldwin GS, Oram M, Erskine SG, Wentzell LM, Szczelkun MD, Nobbs TJ, Halford SE. (1995) A general assay for restriction endonucleases and other DNA-modifying enzymes with plasmid substrates. *Mol. Biotechnol.* **4**:259-268.

Webb MR (2003) A fluorescent sensor to assay inorganic phosphate. In *Kinetic Analysis: A practical Approach*, Johnson KA (ed) pp 131-152. Oxford University Press, Oxford, UK

Webb MR. Development of fluorescent biosensors for probing the function of motor proteins. *Mol. Biosyst.* **3**, 249-256 (2007).

Table S1 Calibration values for the stopped flow ATPase assays as a function of temperature. See **Supp. Methods** and **Fig. S2** for more details.

Temp (º C)	V/μM Pi (±S.E.M.)	Corr Coeff of linear fit	% error	Average % error (±S.D.)
10	2.6075±0.0215	0.9999	0.8	1.4(±0.9)
15	5.7700±0.0520	1.0000	0.9	
20	4.8440±0.1115	0.9995	2.3	
25	3.3430±0.0882	0.9993	2.6	
30	1.9140±0.0096	1.0000	0.5	

Supplementary Figure Legends

Figure S1 Characterisation of the MDCC-PBP preparation used in the phosphate release assays. Fluorescence (λ_{ex} = 430 nm, λ_{em} = 465 nm) was recorded in an HORIBA Jobin Yvon FluoroLog using 5 μM MDCC-PBP in 50 mM Tris-Cl, pH 8.0, 10 mM $MgCl_2$, 1 mM DTT, 20 ºC. The fluorescence with no added P_i is *A*. P_i was then added in 0.5 μM aliquots to 8 μM. A second solution of MDCC-PBP was treated with 2.5 U/ml purine nucleoside phosphorylase and 200 μM 7-methylguanosine for ten minutes, to obtain the "-P_i" fluorescence value (*B*, red line). Linear fits were obtained to the first 7 points (unsaturated MDCC-PBP and up to 3 μM P_i, blue line) and to the last five points (saturated MDCC-PBP, magenta line). *C* gives an estimate of the P_i contamination in the MDCC-PBP sample (~3%). *D* is the effective capacity of the sensor (4.73 μM, ~95%).

Figure S2 Calibration of stopped flow phosphate release assay signal at 10 °C. (**A**) Syringes "C" and "D" were filled with 5 μM MDCC-PBP in 50 mM Tris-Cl, pH 8.0, 10 mM $MgCl_2$, 1 mM DTT. Equal volumes (50 μl) of C and D were mixed and the solution monitored for 60 s. P_i was then added in 0.5 μM aliquots to each syringe and the fluorescence re-measured each time after pushing the new solution into the observation chamber. Each concentration was measured twice (red and black lines). (**B**) The PMT response at each concentration of P_i was calculated from the average of the two traces obtained in **A**. Standard deviations are smaller than the points and are not shown. A linear fit (blue line) gives the linear response of the MDCC-PBP in the stopped flow to changes in P_i concentration. The values obtained at each of the other temperatures are given in **Table S1**.

Figure S3 Comparison of the phosphate release assay and a hand-quenched radioactive assay. For full details of the radioactive assay, see Supplementary Methods; for full details of the phosphate release assay, see the Main Section and Supplementary Methods. ATPase activity was compared using 0.5 nM linear DNA, 60 nM MTase, 200 nM HsdR and 96 μM ATP in Reaction Buffer at 15 ºC. (**A**) Separation of ATP and ADP on two TLC plates (A1-A5 and B1-B3). (**B**) ATP hydrolysed as a function of time was calculated as P_i released using the PBP assay

(red line) or as ADP released using the TLC assay (black circles). The black line shows a fit of the steady-state phase of the P_i data to **Eqn. 3** (see Main Section, Materials and Methods). For the radioactive data, errors in the *y*-axis are the standard deviations from three repeat experiments whilst errors in the *x*-axis show the uncertainty in time accuracy during initiation and quenching (approximated as ±1 s).

Figure S4 Predicted ATPase profiles for EcoR124I. **(A)** A modified version of the model from **Fig. 1A** is shown. This scheme and the kinetic constants are based on a published scheme used to model DNA translocation (Seidel *et al*, 2005). The ATPase kinetics were simulated as previously described using numerical integration in Berkeley Madonna 8.0.1 (http://www.berkeleymadonna.com). The rate constant-dependent production and consumption of each species and hydrolysis of ATP was represented as differential equations. Initial values were equivalent to the experimental conditions as found in the stopped flow immediately upon mixing, namely; M = 0; MR = 1 nM; MT = 0; and R = 199 nM. Dissociation events and ATP hydrolysis during initiation were not considered as they did not effect the kinetic profiles produced (data not shown). **(B)** Simulation of the ATPase kinetics of EcoR124I based on the model in (A). Values for k_{bind}, k_{ini} and k_{off} were taken from translocation data derived previously at 25 ºC (Seidel *et al*, 2005) whilst k_{ATP} was taken as directly proportional to the reported k_{step} values. In addition, we verified that the chosen set of parameters describe well the triplex displacement curves (data not shown), which serves as an independent control for the validity of the model. The example profiles show a slow approach to a linear steady-state. **(C)** Comparison of simulated data from (B) to an equation describing a single exponential approach to a steady-state (Frieden, 1979):

$$y = (V \cdot t) - \left[\left(V \cdot k_1^{-1}\right) \cdot \left(1 - \left(\exp\left(-k_1 \cdot t\right)\right)\right)\right] \qquad \textbf{Equation S1}$$

where V is the steady-state velocity and k_1 is the initial exponential rate. Although this equation can closely describe the model, the significant deviation seen here is due to the influence of k_{off} which causes the MT species to be under-occupied during the steady-state (see **Fig. S6** for further details).

Figure S5 Deviation of the empirical data from a single exponential relationship during initiation. The number of ATP consumed per HsdR as a function of time was calculated from phosphate release data determined using the stopped flow assay at 25 ºC and 1200 μM ATP (open circles; see Main Section). The data has been reduced by three points in every four for clarity. The full data-set was fitted to **Eqn. S1** and residuals calculated using Grafit 5.0.8 (Erithacus software, Staines, UK). The experimental data is well described by **Eqn. S1**. In turn, this shows that the data is also well described by the models in **Figs. 1A** and **S4A**. However, although the residual differences between the data and **Eqn. S1** are small, they show a systematic variation that is indicative of a higher-order exponential relationship during initiation. This is not due to the second-order HsdR binding step – changing k_{bind} does not alter the shape of the initiation phase (data not shown). This indicates that there are either: multiple rate-limiting steps during loop formation whose rates are similar in magnitude; or off-pathway inhibited states during initiation; or an acceleration of the translocation rate as the loop grows beyond a topologically constrained size. Unfortunately, we cannot distinguish between these models from our data.

Figure S6 Occupancy of the translocating species during the steady-state. **(A)** The ATPase kinetics were modelled as in **Fig. S4** using the kinetic values shown which were derived from published values for EcoR124I (Seidel *et al*, 2005) and the initial conditions from **Fig. S4** which represent the conditions used in our experiments. **(B)** The occupancy of the M, MR and MT species as a function of time. When there is no HsdR dissociation, MT becomes fully occupied after 1 s. With k_{off} = 0.1 /s, the value for dissociation of an HsdR from an R_2 complex (Seidel *et al*, 2005), the MT species is ~95% occupied at steady-state with R saturating at 200 nM. We note that the occupancy of the MT species with translocating R is mainly dependent on k_{off} and k_{ini}. Since k_{ini} is much larger than k_{off}, the resulting occupancies are high at saturating R. The obtained occupancy is rather robust, since large changes in the parameters would not describe the triplex displacement curves (e.g. if k_{off} were much larger, processivity would be greatly affected) and/or the ATPase kinetics. For example, if the off rate is increased, then a burst in the steady-state occurs early in the reaction (data not shown). The conditions we chose for our experiments avoided these effects and consequently no evidence of a burst was seen in our ATPase kinetics. **(C)** The

phosphate released during the reaction was calculated for each of the alternatives in part (B) and then fitted to **Eqn. S1** as in **Fig. S5**. Where there is no dissociation of the motor and the MT state is fully occupied, then **Eqn. S1** faithfully returns the kinetic values used in the simulation. Where $k_{off} = 0.1$ /s, the fit returns an apparent value for the steady-state velocity that is ~5% slower than the simulated value in (A). This difference represents the lower occupancy of the MT species during the steady-state – The apparent ATPase rate derived from the linear phase of the profile is proportional to $([MT]/([MT]+[M]+[MR]))\cdot k_{ATP}$.

Figure S7 Arrhenius plots for ATPase activity. Individual data from **Fig. 3A**. Temperature dependence of the rate of ATP hydrolysis at ATP concentrations 12.5, 25, 48, 96, 170 320 600 and 1200 μM. The $V_{max,calc}$ data was obtained from the hyperbolic fits in **Fig. 1E**. Solid lines represent independent fits to **Eqn. 1**.

Figure S8 Arrhenius plots for translocase activity. Individual data from **Fig. 3A**. Temperature dependence of the rate of translocation at ATP concentrations 12.5, 25, 48, 96, 170 320 600 and 1200 μM. The $V_{max,calc}$ data was obtained from the hyperbolic fits in **Fig. 2C** and Seidel et al., (2005). Solid lines represent independent fits to **Eqn. 1**.

Figure S9 Fitting the single molecule R_1 translocation velocity data (**Fig. 4C**) assuming two rate-limiting steps with a different temperature dependence. (**A**) The blue line is a fit of the data, where one rate was assumed to be dependent on temperature and the other rate to be independent on temperature. Both rates were assumed to be equal at 25 °C. The red line is a single exponential fit as in **Fig. 4C**. (**B**) Fits to the data, where both rate limiting steps are temperature dependent, but are different in that dependency. Both rates were assumed to be equal at 25 °C and the difference between the activation energies was set to a fixed value, whereas all the pre-exponential factors and the activation energies were subjected to the fit. Two fits for activation energy differences ΔΔG of 10 and 30 k_BT are shown. Even for ΔΔG of 10 k_BT a single exponential fit provides the better description.

Figure S10 Comparison of translocase data from ensemble and single molecule assays. For the tweezers data: The R_1 rate data was taken directly from **Fig. 4C;** The R_2 rate in **Fig. 4C** represents the additive translocation rate of two divergent HsdR motors and so was halved to estimate the rate of one HsdR motor (this assumes that the motors are independent, as has been demonstrated previously – Firman and Szczelkun, 2000; Seidel et al., 2004; 2005). For the triplex data: to compare with the tweezers data taken at 4 mM ATP, $V_{max,calc}$ data was taken from the fits in **Fig. 2C**. The combined data was then fitted to **Eqn 1**.

Figure S1

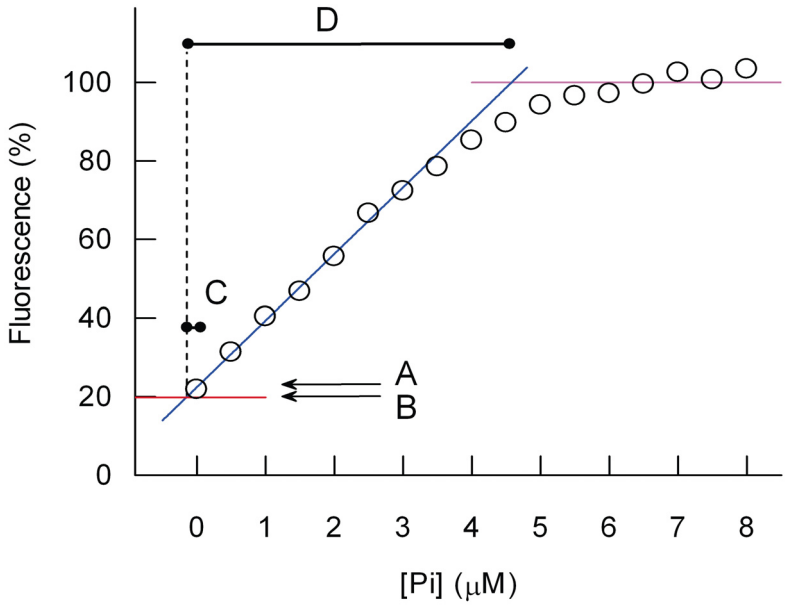

Figure S2

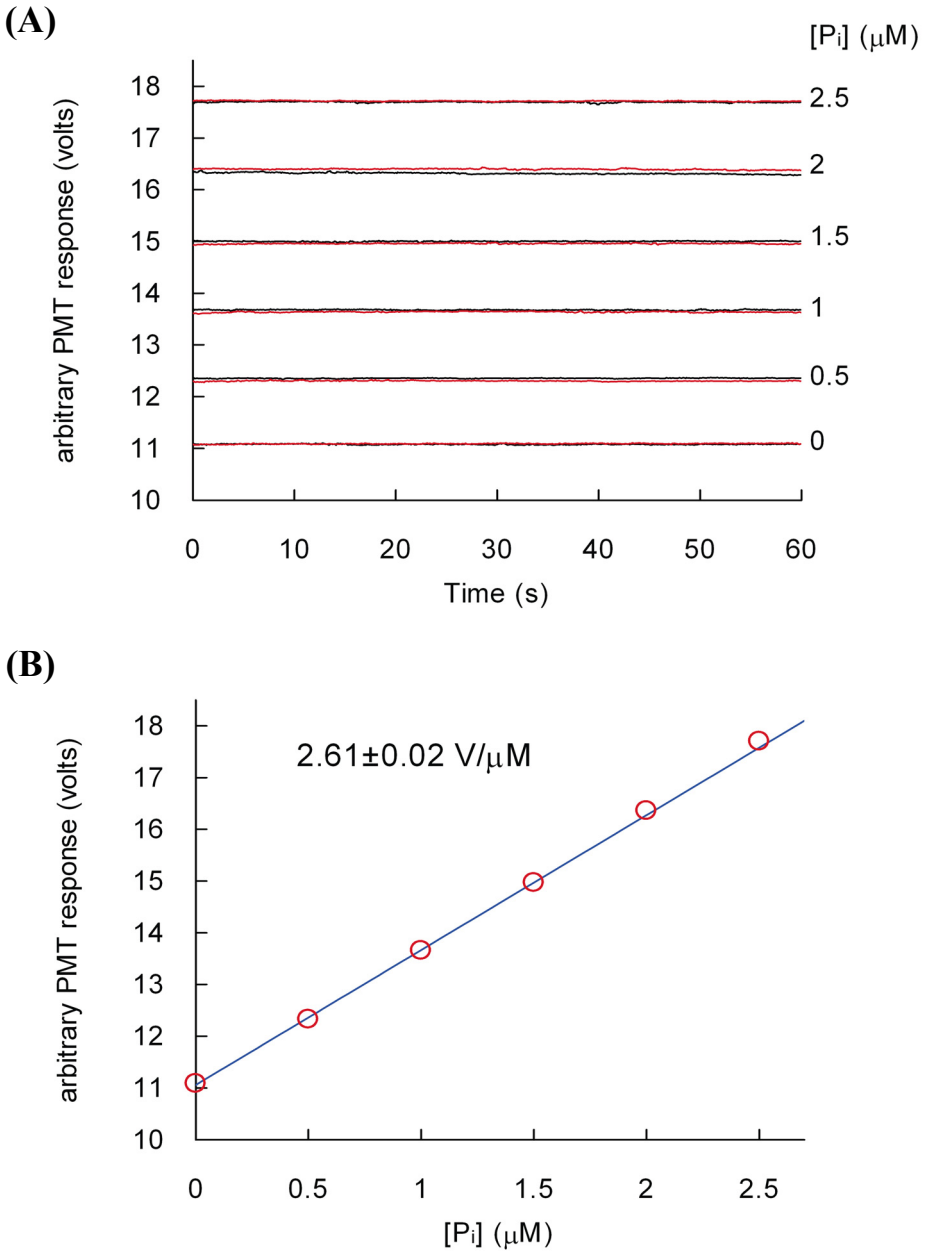
(A)
[Pi] (μM)
2.5
2
1.5
1
0.5
0
arbitrary PMT response (volts)
18
17
16
15
14
13
12
11
10
0
10
20
30
40
50
60
Time (s)
(B)
2.61±0.02 V/μM
arbitrary PMT response (volts)
18
17
16
15
14
13
12
11
10
0
0.5
1
1.5
2
2.5
[Pi] (μM)

Figure S3

(A)

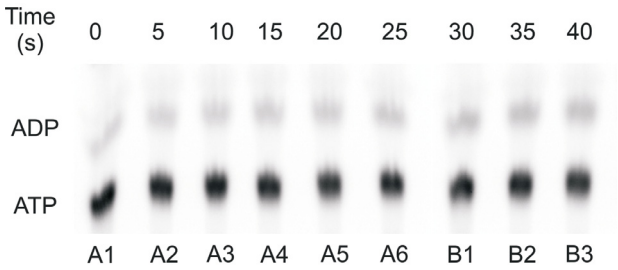
Time (s)
0
5
10
15
20
25
30
35
40
ADP
ATP
A1
A2
A3
A4
A5
A6
B1
B2
B3

(B)

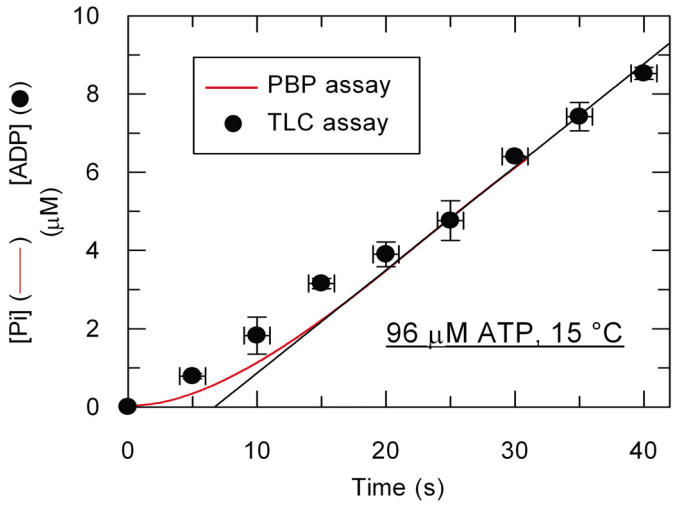
[Pi] (—) [ADP] (●) (μM)
PBP assay
TLC assay
96 μM ATP, 15 °C
Time (s)
0
2
4
6
8
10
0
10
20
30
40

Figure S4

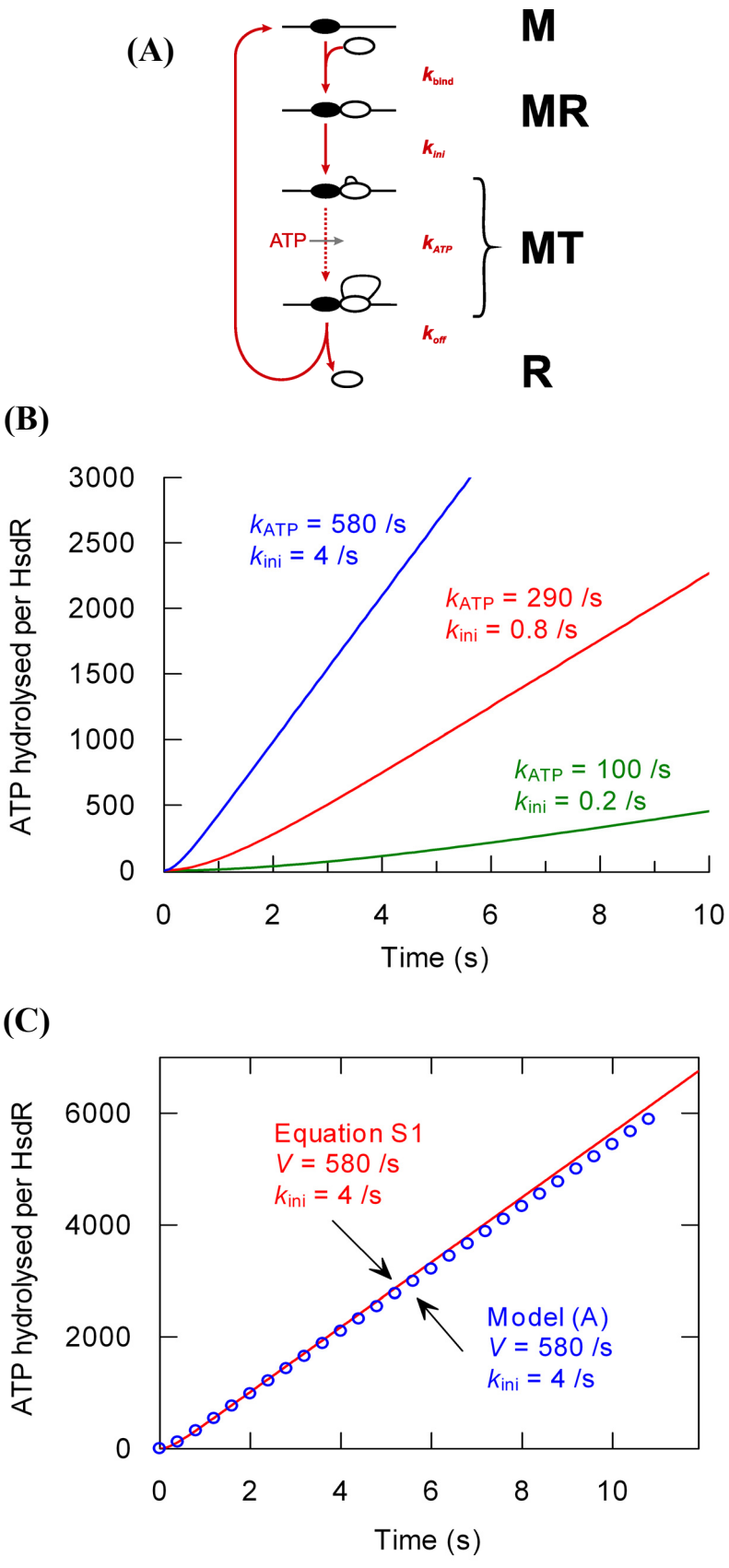
(A)
M
MR
MT
R
ATP
k_{bind}
k_{ini}
k_{ATP}
k_{off}
(B)
ATP hydrolysed per HsdR
Time (s)
k_{ATP} = 580 /s
k_{ini} = 4 /s
k_{ATP} = 290 /s
k_{ini} = 0.8 /s
k_{ATP} = 100 /s
k_{ini} = 0.2 /s
(C)
ATP hydrolysed per HsdR
Time (s)
Equation S1
V = 580 /s
k_{ini} = 4 /s
Model (A)
V = 580 /s
k_{ini} = 4 /s

Figure S5

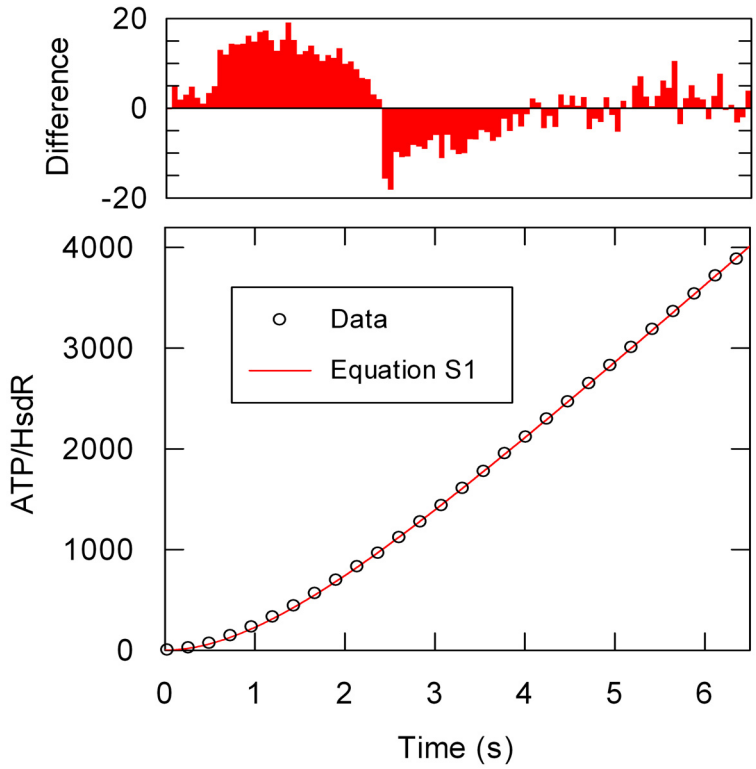
Difference
20
0
-20
ATP/HsdR
4000
3000
2000
1000
0
Data
Equation S1
0
1
2
3
4
5
6
Time (s)

Figure S6

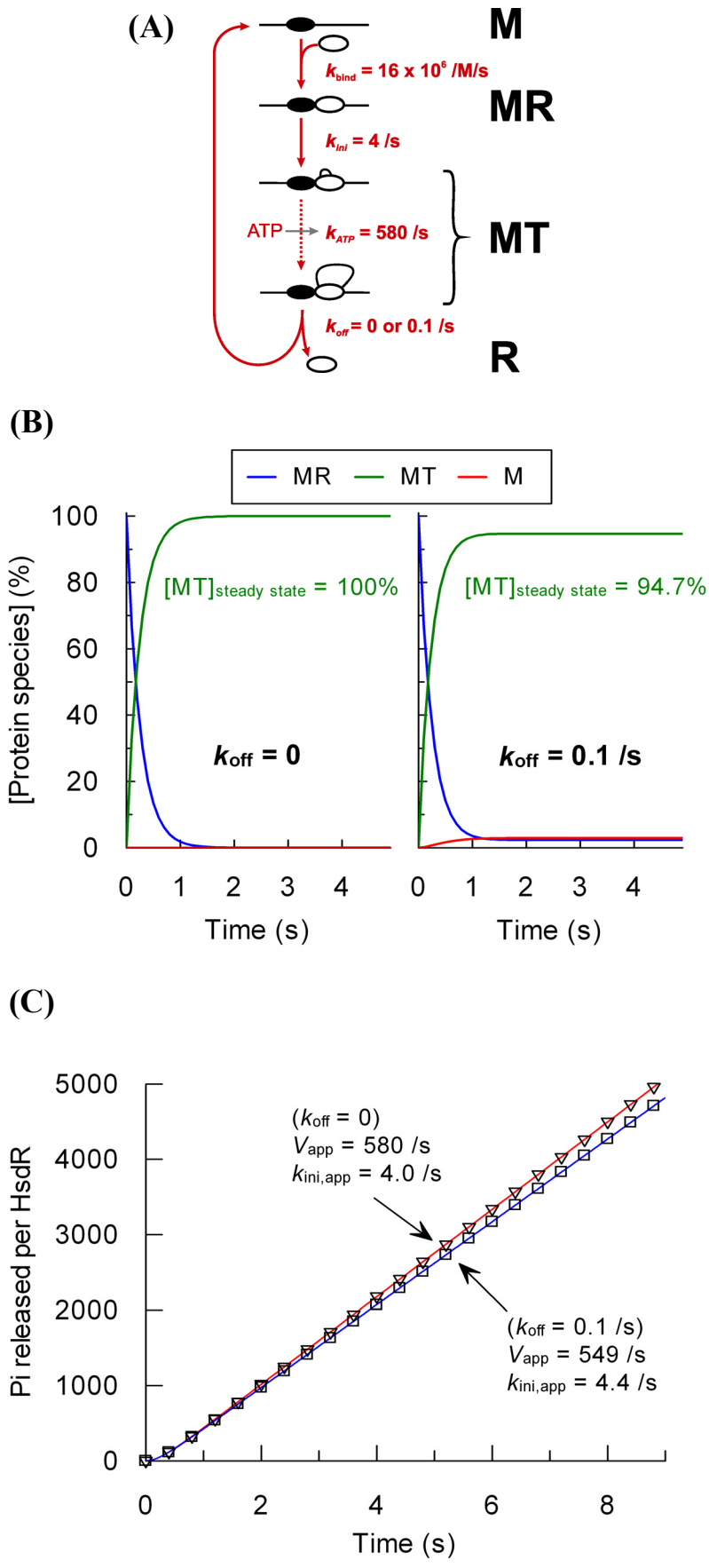
(A)
M
k_{bind} = 16 x 10^6 /M/s
MR
k_{ini} = 4 /s
ATP
k_{ATP} = 580 /s
MT
k_{off} = 0 or 0.1 /s
R
(B)
MR
MT
M
[Protein species] (%)
100
80
60
40
20
0
[MT]steady state = 100%
[MT]steady state = 94.7%
k_{off} = 0
k_{off} = 0.1 /s
0 1 2 3 4
Time (s)
0 1 2 3 4
Time (s)
(C)
Pi released per HsdR
5000
4000
3000
2000
1000
0
(k_{off} = 0)
V_{app} = 580 /s
$k_{ini,app}$ = 4.0 /s
(k_{off} = 0.1 /s)
V_{app} = 549 /s
$k_{ini,app}$ = 4.4 /s
0 2 4 6 8
Time (s)

Figure S7

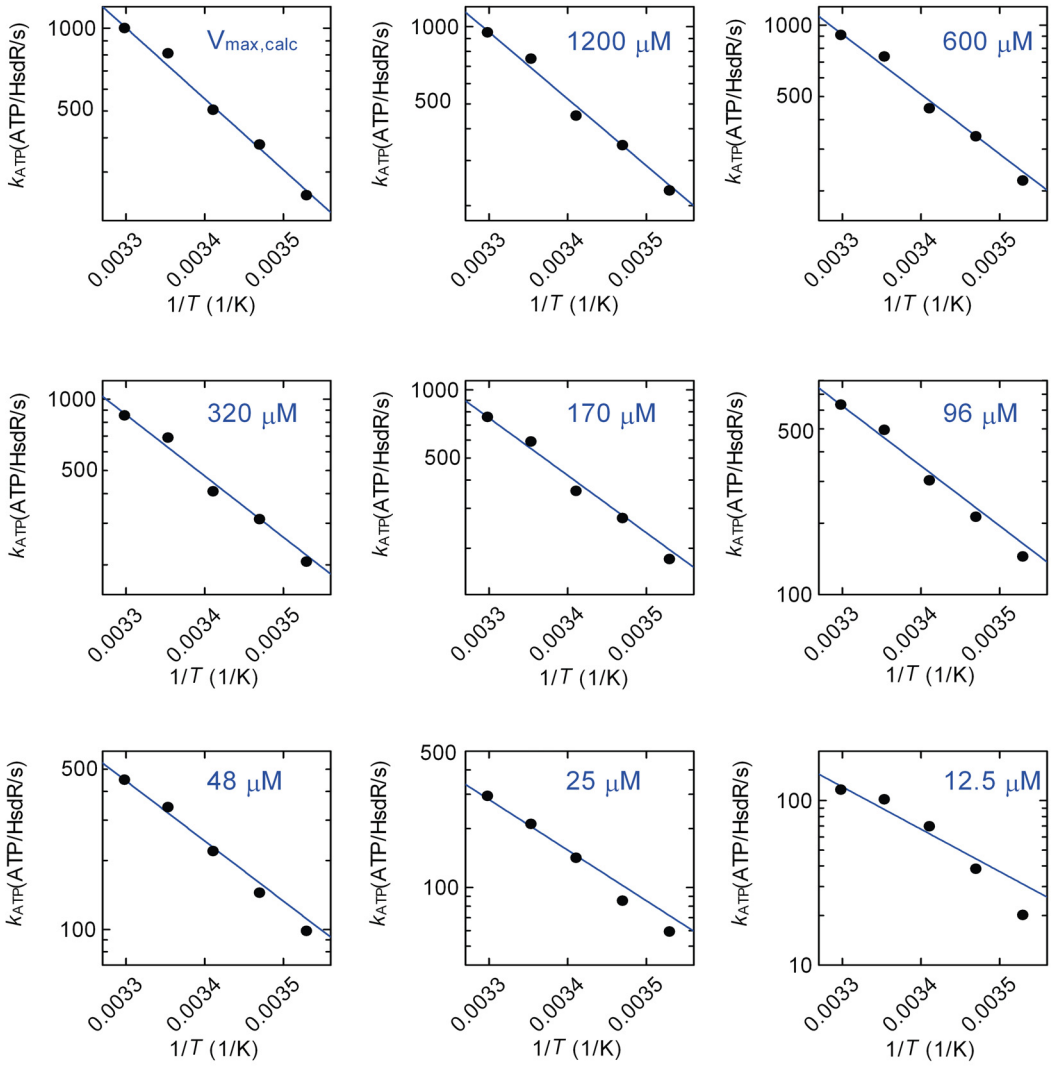
k_{ATP}(ATP/HsdR/s)
1000
500
$V_{max,calc}$
0.0033
0.0034
0.0035
1/T (1/K)
1200 μM
600 μM
320 μM
170 μM
96 μM
100
48 μM
25 μM
12.5 μM
10

Figure S8

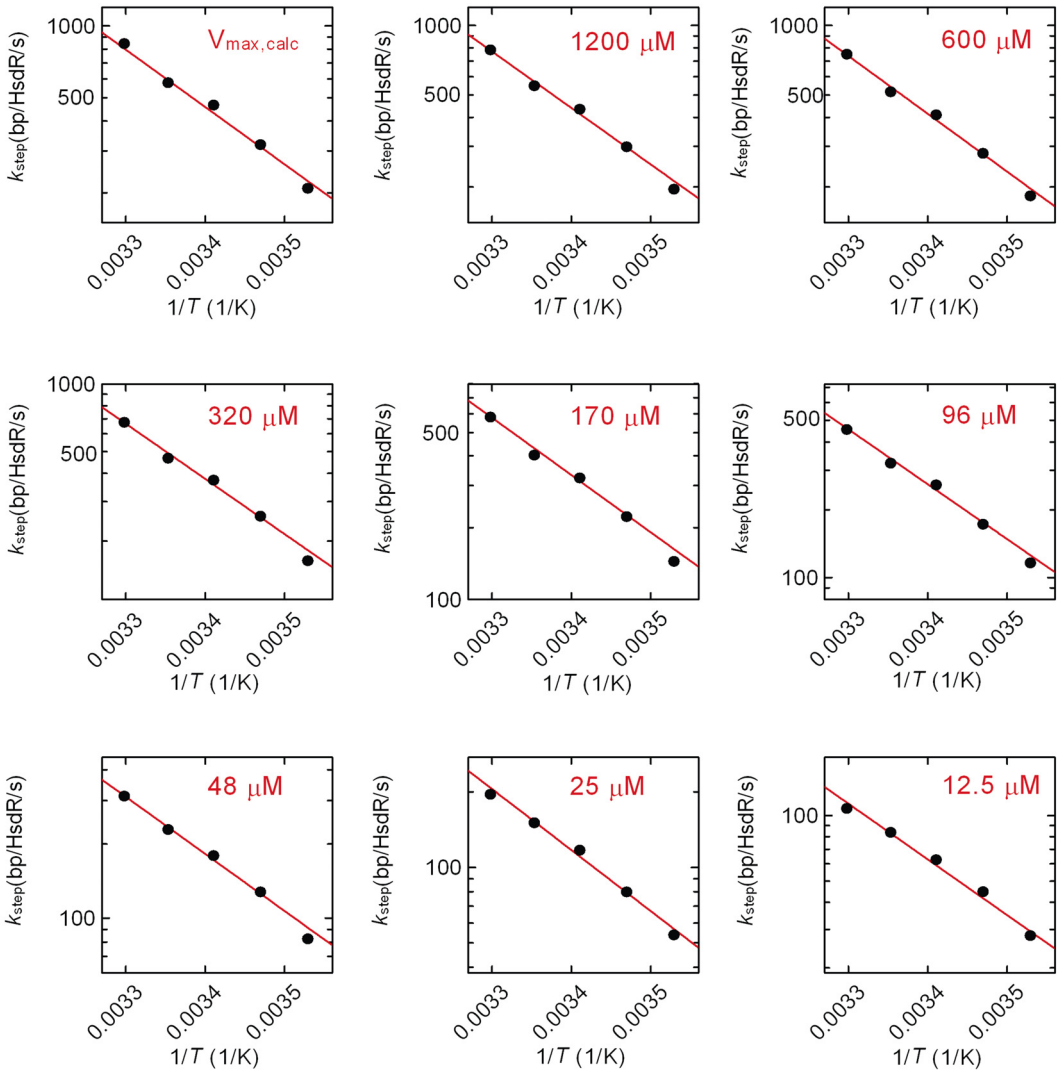
$V_{max,calc}$
1200 μM
600 μM
320 μM
170 μM
96 μM
48 μM
25 μM
12.5 μM
k_{step}(bp/HsdR/s)
1/T (1/K)
0.0033
0.0034
0.0035
1000
500
100

Figure S9

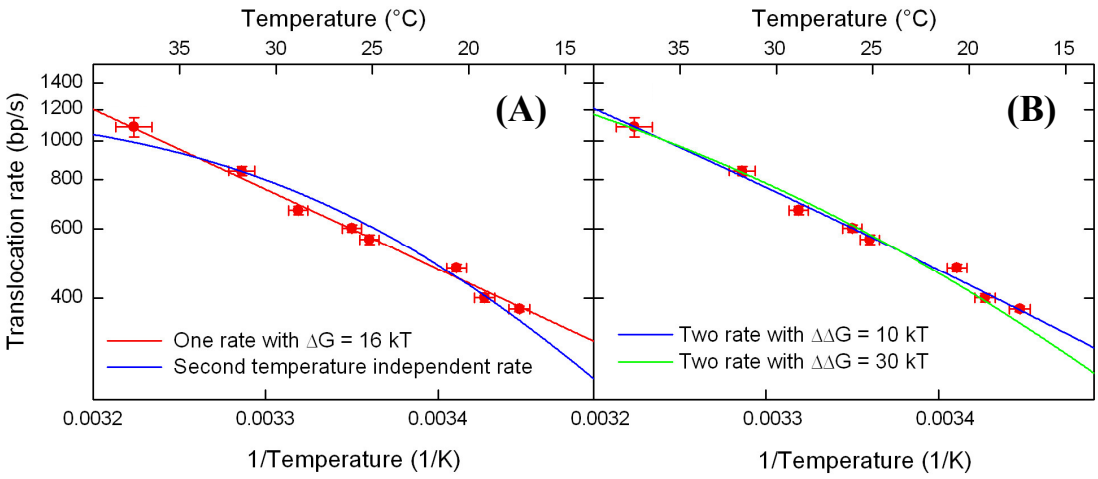
Temperature (°C)
35
30
25
20
15
Translocation rate (bp/s)
1400
1200
1000
800
600
400
(A)
One rate with ΔG = 16 kT
Second temperature independent rate
0.0032
0.0033
0.0034
1/Temperature (1/K)
(B)
Two rate with ΔΔG = 10 kT
Two rate with ΔΔG = 30 kT

Figure S10

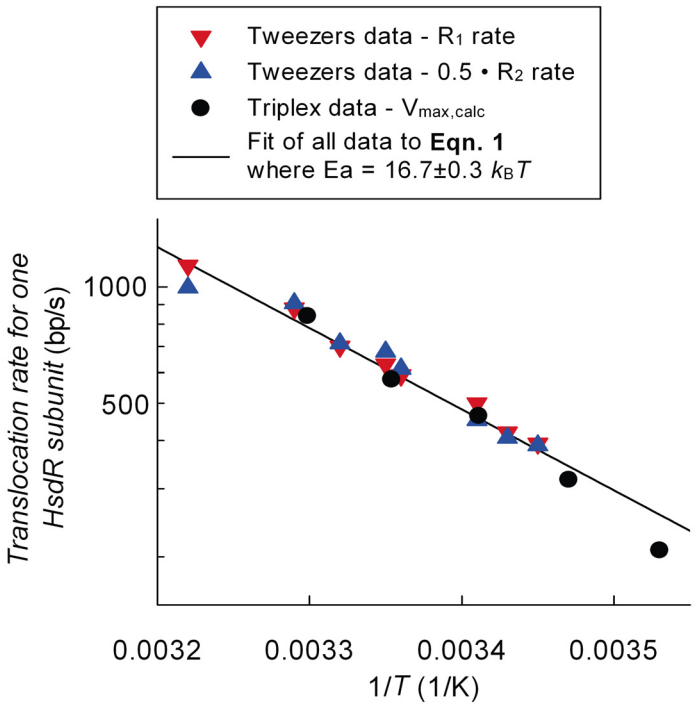
Tweezers data - R1 rate
Tweezers data - 0.5 • R2 rate
Triplex data - Vmax,calc
Fit of all data to Eqn. 1
where Ea = 16.7±0.3 kBT
Translocation rate for one HsdR subunit (bp/s)
1000
500
0.0032
0.0033
0.0034
0.0035
1/T (1/K)